Parametric studies on the flow characteristics in porous media for the development of indicator predicting shelf life of perishable food items

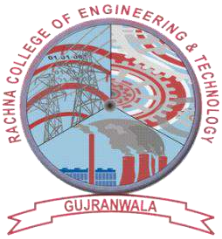

By

Syed Rehman Jamil	2019-ME-443
Shahid Sarwar	2019-ME-446
Hammad Qureshi	2019-ME-449

Research Supervisor:

Dr. Salman Abbasi

2023

Mechanical Engineering Department

Rachna College of Engineering and Technology
Gujranwala

(A Constituent College of University of Engineering and Technology Lahore)

Parametric studies on the flow characteristics in porous media for the development of indicator predicting shelf life of perishable food items

Syed Rehman Jamil 2019-ME-443

Shahid Sarwar 2019-ME-446

Hammad Qureshi 2019-ME-449

A THESIS

presented to the Rachna College of Engineering and Technology Gujranwala

in partial fulfillment of the requirements for the degree of

Bachelor of Science

in

Mechanical Engineering

APPROVED BY:

[Primary Advisor/Internal Examiner]	[External Examiner]
[Official Title & Department]	[Official Title & Department]

[Chairman of the Department]

May 2023

Department of Mechanical Engineering

RACHNA COLLEGE OF ENGINEERING AND TECHNOLOGY GUJRANWALA

ACKNOWLEDGMENT

The research project tittled “Parametric studies on the flow characteristics in porous media for the development of indicator predicting shelf life of perishable food items” was successfully completed in the Mechanical Engineerng Department (RCET) of the University of Engineering and Technology, Lahore under the Pakistan Engineering Council (PEC) Annual Award of Final Year Design Project (FYDPs) for the year 2022-2023. The project was supervised by Dr. Muhammad Salman Abbasi.

STATEMENT OF ORGINALITY

It should be noted that the research work in this article is based on my own ideas and research work. Contributions and ideas of others are welcome and included in the article. This article was written by us.

[Syed Rehman Jamil

Shahid Sarwar

Hammad Qureshi]

Table of Contents

List of Figures

List of Tables

Chapter 1

Microfluidic Paper-Based Analytical Devices

Abstract

In this chapter, we briefly present a review on different microfluidic paper based analytical devices (μPADs). We discuss the underlying basic theory controlling the working of these devices. Moreover, different designs of μPADs along with their fabrication methods and potential applications are also discussed.

1.1 Introduction

The use of advanced technologies and materials in packaging to provide additional functionality beyond traditional containment and protection is referred to as intelligent packaging, also known as smart packaging. It includes features that interact with the product, the environment, or the users, allowing for improved safety, quality monitoring, information sharing, and user engagement. The packaging industry has become a significant and rapidly expanding commercial sector globally, primarily driven by the substantial demand for packaging materials in the food and other industries. The market value of intelligent packaging was approximately 13.6 billion USD at the end of 2023, and it is increasing at a CAGR (compound annual growth rate) of 6.5%. Based on the "Fortune Business Insights" Research Report, the worldwide food packaging industry was valued at approximately $400 billion in 2018. It is projected to grow at a compound annual growth rate of 5.6% and is expected to reach approximately $600 billion by 2026 [1]–[3].

In simple terms, when we talk about shelf life, it means how long food can stay safe and good to eat. People usually rely on the expiration dates mentioned on food packages to decide if the food is still alright to consume. These dates are just estimates based on specific temperature conditions. But here's the catch: temperature can vary a lot during the transportation and storage of food, and it greatly affects how long the food stays fresh. So, temperature plays a crucial role in determining the actual shelf life of food from the time it is made until it reaches your plate [4]. The expiration dates printed on food packages may not accurately indicate the quality and safety of the food for consumers. So, to solve these issues Flexible Time Temperature Indicators (FTTI’s) are used and their demand is increasing day by day after new chronic epidemic. A time-temperature indicator is a device or label that provides information about the temperature history of a product over time. It helps to monitor and track the conditions to which a product has been exposed, specifically regarding temperature. It is a simple tool that changes color or shows visual cues to indicate if the product has been subjected to temperatures that might affect its quality or safety. Time-temperature indicators are helpful in ensuring that perishable goods, such as food or pharmaceuticals, have been stored and transported under suitable temperature conditions, thus providing a better indication of their freshness and safety for consumers [5].

Time Temperature Indicators (TTIs) can be divided into two types: partial history indicators and full history indicators, based on how they work. Partial history indicators only show a response when a certain temperature limit is surpassed, whereas full history indicators respond regardless of any temperature threshold being crossed [6]. Time-Temperature Indicators can be grouped into four main categories based on how they work. These categories include biological, chemical, enzymatic, and physical TTIs [7]. An effective Time-Temperature Indicator (TTI) should exhibit a continuous, measurable, and irreversible change in response to temperature. This change should accurately reflect the degree of food quality deterioration and remaining shelf life. Consistency is key, as the TTI should consistently respond in the same manner when exposed to identical temperature conditions. Additionally, it should be cost-effective and versatile enough to accommodate various temperature ranges, with response periods ranging from days to over a year. Practicality matters too, with a small size that allows for easy integration into food packaging and compatibility with high-speed packaging processes. Long shelf life before activation and simple activation procedures are desirable features. The TTI should remain unaffected by factors like light, humidity, and air pollutants, while also enduring normal handling without altering its response. Safety is paramount, making non-toxicity essential. Clear communication is important, ensuring that the TTI effectively conveys its intended message to stakeholders in a straightforward manner. Lastly, visual understandability and adaptability for electronic measurement facilitate easier information storage and utilization [8].

Capillary penetration in porous materials is a concept that finds its use in various industries like textiles, ceramics, printing, and pharmaceuticals. Lately, there has been a rise in the development of diagnostic tests and rapid methods that make use of porous materials and the principles of capillary penetration [7]. Porous materials are used to make microfluidic paper-based analytical devices. A paper-based microfluidic device, in scientific terms, refers to a miniaturized system that utilizes paper as the primary substrate for controlling the flow of fluids at a small scale. It involves the fabrication of channels, typically made of cellulose-based paper, which enable the manipulation and transport of liquids and analytes in a controlled manner. These devices leverage the capillary action of paper to facilitate fluid movement without the need for external pumps or power sources. The paper

acts as a platform for performing various analytical and diagnostic tests, offering advantages such as low cost, simplicity, portability, and ease of use [9], [10]. Microfluidic paper-based analytical devices (μPADs) have diverse applications in healthcare, environmental monitoring, food safety, and bioanalytical research. In healthcare, μPADs enable rapid and low-cost diagnostics for infectious diseases. In environmental monitoring, they detect heavy metals and pollutants in water sources. For food safety, μPADs detect contaminants in food samples, ensuring supply chain safety. In bioanalytical research, μPADs enable DNA analysis, protein detection, and enzyme assays with miniaturization and high-throughput capabilities. These devices offer simplicity, affordability, portability, and ease of use, making them valuable tools for point-of-care diagnostics and resource-limited settings [10], [11].

1.2 Background

Paper-based microfluidic analytical devices (μPADs) are portable and low-cost devices that combine microfluidic principles with paper substrates to perform a variety of analytical tests. Microfluidic paper-based analytical devices (μPADs) have gotten a lot of attention in analytical chemistry because of their advantages over traditional methods, such as low cost of production, flexibility, operational simplicity, trivialize, compatibility with biomolecules, high speed, point-of-care detection, and low reagent consumption [11], [12]. μPADs offer a different platform for liquid transport via capillary forces, eliminating the need for external pumps [13]. Additionally, multiplexed analysis can be performed simply by adding channels.

The working principle of a μPADs is capillary action, in which fluids flow through the paper due to the material's wicking properties. Typically, a small volume of the liquid sample is introduced at the designated inlet area. Capillary action then spreads the sample along the hydrophilic channels, coming into contact with reagents or sensing elements confined on the paper [12], [14].

1.3 A Brief History of Microfluidic Paper-Based Analytical Devices

For many centuries, paper has been employed in chemical measurements, dating back to the use of litmus paper to determine pH levels [15]. The initial bioactive paper for glucose

analysis in urine was developed by Comer [16]. Paper was employed for chromatography purposes for a considerable duration [17]. In the realm of molecular detection, a significant advancement occurred with the introduction of lateral flow assays (LFAs) during the 1970s. Lateral flow assays (LFAs) commonly capture labeled antibodies and employ visual observation of a colored band to qualitatively detect signature molecule. Lateral flow assays (LFAs) have found applications in various domains such as medicine, food science, environmental monitoring, and biodefense and their applications are increasing day by day [18]. The field of paper-based microfluidics gained significant attention after the publication of the first μPAD by the Whitesides group, which utilized photolithography as the method for creating patterns [11]. Microfluidic paper-based analytical devices (μPADs) distinguish themselves from LFAs and litmus paper by employing chemical printing and cutting techniques to create flow channels, enabling the performance of multiplexed analysis with minimal sample volumes. Various fabrication techniques, including photolithography [19], plasma treatment [20], wax printing [21], plotting [22], wax dipping [23], inkjet printing [24], flexographic printing [25], laser treatment [26], and stamping [27], have been shown to be effective in producing microfluidic paper-based analytical devices (μPADs). All fabrication techniques are used today for producing microfluidic paper-based analytical devices (μPADs) but all have their own pros and cons.

1.4 Fabrication

The fabrication of microfluidic devices involves selecting a suitable porous membrane that meets specific criteria, including thickness, pore distribution, price, and absorption rate. The choice of membrane substrate is crucial, and the properties of the paper should be carefully evaluated for optimal device construction. To create hydrophobic barriers, the hydrophilic membrane is patterned, enabling controlled flow of samples through isolated regions. Different techniques, such as photolithography [28], printing [24], cutting [29], and chemical vapor deposition [30], have been employed to define these hydrophobic barriers. In this chapter we discuss only cutting technique that is used in the fabrication of microfluidic paper-based analytical devices (μPADs).

1.5 Cutting

Fabricating channels out of paper through paper cutting is considered one of the simplest and oldest techniques. In the process of fabricating microfluidic paper-based analytical devices (µPADs), the paper substrate is intricately patterned into a network of interconnected channels and zones. This is achieved through the utilization of precise and programmable tools such as a knife cutter (vinyl plotter) or a laser cutter (CO_2 laser). Alternatively, though less refined, manual cutting methods involving scissors or a knife can also be employed to generate rudimentary devices. To confer structural stability to the paper-based devices, it is common practice to employ tape or glass slides as protective encasements. The cutting technique presents notable advantages, as it circumvents the need for chemical treatments and can be executed using rudimentary tools like scissors or razor blades. However, due to the nature of channel excision, the resulting devices exhibit increased handling challenges, necessitating the utilization of a sturdy support structure to ensure mechanical integrity and stability of the channels [31]–[34].

In a recent scientific investigation, researchers outlined a parafilm-based cutting technique. This approach involves the initial fusion of paper and parafilm through the application of heat and pressure using a hot press. As a result, two distinct types of fused structures are formed: laminated paper (referred to as l-paper) and infused paper (known as i-paper). The fusion process can be either partial or complete, determining the extent to which the two layers are combined [35].

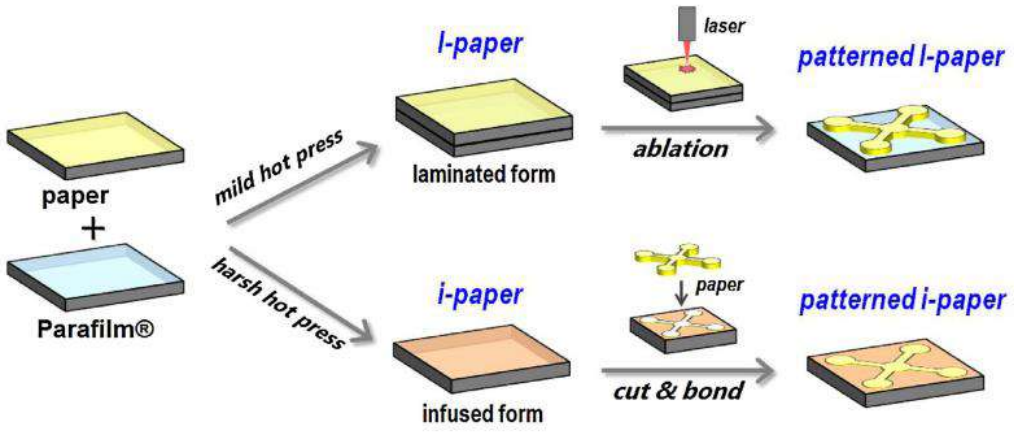

Figure 1.1: Patterning paper using Para film [58]

1.6 Applications of Microfluidic Paper-Based Analytical Devices

μPADs have found usage in a variety of applications due to their inherent advantages of speed, low cost, ease of use, and disposability. Much of the early research focused on medical applications and global health, but a variety of other fields emerged, including food safety, environmental monitoring, and forensics [36]. Microfluidic Paper-based analytical devices (μPADs) have gained significant attention in the field of medicine and healthcare. Pregnancy tests are widely recognized as one of the prominent applications of μPADs. A novel paper-based analytical device was developed by Noiphung et al. [37] for the determination of blood type. In emergency situations or resource-limited settings, paper-based blood typing assays have been developed as valuable tools for determining an individual's blood type (A, B, AB, or O) utilizing minimal blood samples [38]. Due to its potential impacts on human, plant, and animal well-being, environmental pollution has become a growing concern that necessitates comprehensive monitoring efforts. μPADs offer an alternative analytical technique to traditional methods that are inexpensive, effective, and suitable for in-field analysis of environmental pollutants [39]. The safety of food and water can be compromised by various factors, such as the introduction of pathogens, pesticides, herbicides, metals, and other toxic substances, which are typically associated with agricultural and industrial activities. Additionally, the utilization of food additives for purposes such as preservation, coloring, and sweetening can also influence the safety of food and water [40]. Microfluidic paper-based analytical devices (μPADs) designed for pathogen detection in food have predominantly relied on enzymatic assay-based optical techniques. These methods involve the visualization of results through visual confirmation by human observation or digital conversion of images, followed by measurement using image analysis software. These devices are also used for detecting additives, heavy metals and contaminants in water and food [41]. Microfluidic paper-based analytical devices (μPADs) are also employed to check the time and temperature history of food and perishable products.

1.7 Darcy's law

Henri Darcy [42], a French engineer, developed a mathematical relationship known as Darcy's law in 1856. It controls the flow of groundwater through granular media and the movement of other fluids through porous materials, such as petroleum through rocks. Darcy's law has been derived from Navier-Stokes equation [43] via homogenization method [44]. Morris Muskat [45], an American petroleum engineer made a significant contribution by refining Darcy's equation, originally proposed by Henry Darcy, to specifically address single-phase flow characteristics. Muskat's refinements ensured its applicability to the unique challenges encountered in petroleum engineering. Building upon the experimental findings of his colleagues, Muskat collaborated with Milan W. Meres to further extend the scope of Darcy's law. Their work resulted in a generalization of the law, encompassing the intricate multiphase flow phenomena involving water, oil, and gas within the porous medium of petroleum reservoirs.

Darcy's law is a fundamental principle in fluid dynamics that describes the flow of fluids through porous media. Darcy's law states that, "the flow rate (q) of a fluid through a porous medium is directly proportional to the pressure gradient (Δp) across the porous media and inversely proportional to length (L) of media and the fluid's dynamic viscosity (μ).

Mathematically, it can be expressed as:

$$q = \frac{K(\Delta p)}{\mu L} \tag{1.1}$$

Where:

q= Flow rate of fluid in porous media

k= Permeability of porous media

Δp= Pressure gradient across the ends

μ= Dynamic viscosity of fluid

L= Length of porous material

This can be illustrated with the figure given below:

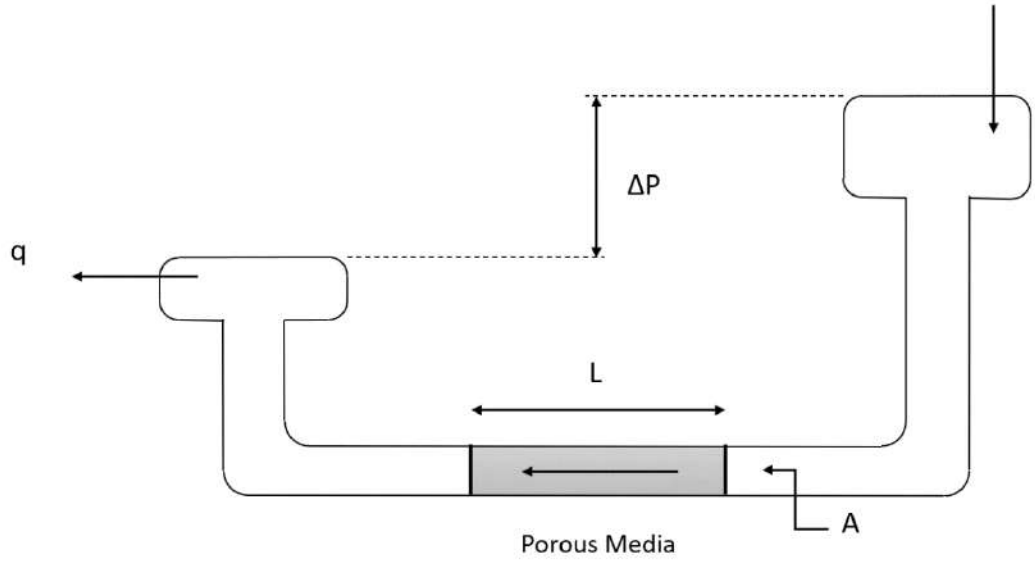

Figure 1.2: Darcy's law notations

Darcy's law assumes that the fluid flow is steady, laminar, and incompressible. It is applicable to both single-phase and multiphase flows, although modifications and extensions may be required for multiphase scenarios.

Darcy's law provides a foundational framework for analyzing and predicting fluid flow in various natural and engineered systems, such as groundwater flow in aquifers, oil and gas reservoirs, and geotechnical engineering applications involving soil permeability.

1.8 Permeability of Fluid

The ability of a fluid (such as a gas or a liquid) to pass through a porous material or medium is referred to as permeability. It's a property that describes how easily a fluid can move through a substance or medium [46].

Permeability in porous materials is determined by the structure and properties of the material itself. Porous materials have interconnected void spaces, or pores, that allow fluids to flow through them. The permeability of a material is affected

by the size, shape, and distribution of its pores [47]. Permeability is generally higher in materials with larger and more interconnected pores. Permeability is the proportionality constant represented by K in Darcy's Law.

$$K = \frac{q\mu L}{\Delta p} \quad \textbf{(1.2)}$$

Several factors control the permeability of a fluid through a porous medium. These factors include:

- **Pore Size and Distribution:** The size, shape, and distribution of pores within the medium all influence permeability. Larger and more interconnected pores facilitate fluid flow, resulting in higher permeability. Smaller or poorly interconnected pores, on the other hand, can restrict fluid movement and result in lower permeability.
- **Porosity:** The volume fraction of void spaces or pores within a porous medium is referred to as porosity. Because there is more volume available for fluid flow, higher porosity generally corresponds to higher permeability. It is important to note, however, that the relationship between porosity and permeability can be complicated, as pore size and distribution also play a role.
- **Viscosity:** The viscosity of the fluid passing through the medium influences its ability to flow. Fluids with a higher viscosity resist flow more and may have a lower permeability. Fluids with lower viscosity, on the other hand, flow more easily and have higher permeability.
- **Saturation:** The degree to which the pore spaces within the porous medium are filled with fluid is referred to as saturation. The saturation level of a fluid influences its permeability, as higher saturation levels generally correspond to higher permeability. The relationship between saturation and permeability, on the other hand, can be nonlinear, especially in multiphase flow systems.
- **Grain Size and Shape:** The size and shape of the solid grains that make up the porous medium can have an effect on permeability. Permeability is

generally higher in materials with larger grain sizes or more rounded grains. Irregularly shaped or smaller grains can cause fluid flow to take more tortuous paths, lowering permeability.

1.9 Dynamic Viscosity of Fluid

Dynamic viscosity, often known as viscosity, is an essential property of a fluid that defines its resistance to flow under shear stress. It quantifies the internal friction of a fluid when neighboring layers slide past each other. When a force is applied to a fluid, such as by passing a solid object through it or applying pressure on it, the fluid's layers experience relative motion. The dynamic viscosity quantifies the amount of internal friction that resists relative motion and dictates how easily the fluid flows.

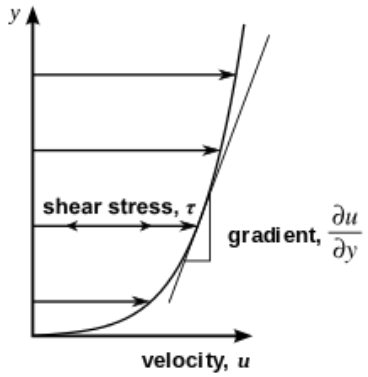

Figure 1.3: Boundary layer on a flat plate [48]

Newton's law of viscosity [49] describes the link between shear stress and dynamic viscosity in the context of a boundary layer on a flat plate. The shear stress (τ) within a fluid is directly proportional to the dynamic viscosity (μ) and the velocity gradient (du/dy) perpendicular to the direction of flow, according to Newton's law:

$$\tau = \mu \frac{du}{dy} \tag{1.3}$$

where:

- τ represents the shear stress (force per unit area) exerted on the fluid in the direction perpendicular to the flow.

- μ denotes the dynamic viscosity of the fluid.
- (du/dy) represents the velocity gradient, which is the change in velocity (du) per unit distance (dy) perpendicular to the direction of flow.

The frictional forces between the fluid layers within the boundary layer are the ones that cause the shear stress to form in the boundary layer on a flat plate. A velocity gradient is produced as a result of the fluid's changing velocity within the boundary layer as it moves along the plate. The fluid experiences shear stress as a result of this velocity gradient.

1.10 Lucas-Washburn Equation

The Lucas-Washburn equation is an empirical relationship that describes the time-dependent penetration of a liquid through a porous medium. Richard Lucas [50] developed it in 1921, and Edward Wight Washburn [51] refined it in 1928. The equation approximates the capillary flow [52] of a liquid through a narrow tube or porous material.

The Lucas-Washburn equation is used to describe the length of fluid imbibition in capillary or porous media as a function of diffusion co-efficient and time period during which wicking is permitted.

Lucas-Washburn Equation states that: "The rise of fluid in a capillary is proportional to the square root of the capillary's radius, the time period of wicking, and fluid properties such as contact angle and surface tension, and inversely proportional to the fluid's dynamic viscosity."

The mathematical form of Lucas-Washburn Equation is given as

$$L^2 = \gamma \frac{rtcos\theta}{2\mu} \quad \textbf{(1.4)}$$

L= Rise of fluid in capillary

Θ= Contact Angle of fluid

ϒ= Surface tension of fluid

μ= Dynamic Viscosity

r= Radius of Capillary tube

t= Time period of imbibition

1.11 Capillary Action

Capillary action is the phenomenon in which a liquid is drawn into a narrow tube or porous material against the force of gravity. It happens as a result of the interaction of adhesive and cohesive forces within the liquid and between the liquid and the solid surfaces. The balance between cohesive forces, which cause molecules within the liquid to attract each other, and adhesive forces, which cause molecules of the liquid to adhere to the solid surface, can explain the process of capillary action. The liquid rises in the capillary tube or porous material when the adhesive forces between the liquid and the solid surface are greater than the cohesive forces within the liquid [53], [54].

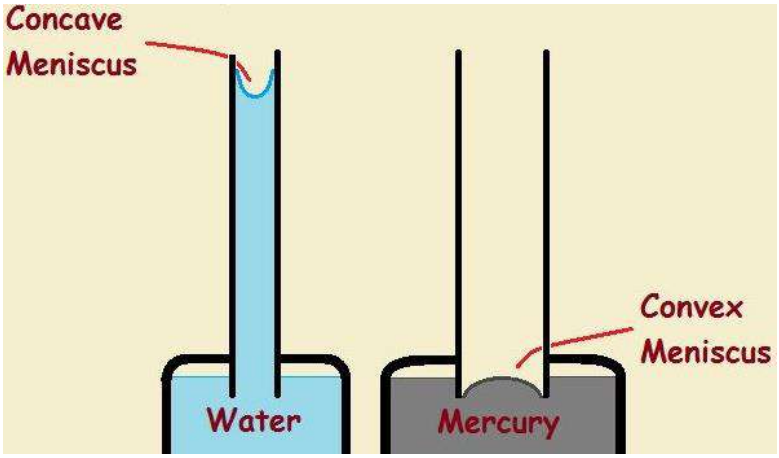

Figure 1.4: Capillary action of different liquids [55]

The mathematical relation of capillary action is often described by the Lucas-Washburn equation, which quantifies the rate of liquid absorption into a capillary tube or porous material over time. The equation is as follows:

$$h = \frac{2\gamma \cos\theta}{\rho g r} \quad \textbf{(1.5)}$$

In this equation:

2. **h** represents the increase in height of the liquid column over time (in meters).
3. **γ** is the surface tension of the liquid (in newtons per meter).
4. **θ** is the contact angle between the liquid and the solid material (in degrees).
5. **ρ** is the density of the liquid (in kilograms per cubic meter).
6. **g** is the acceleration due to gravity (in meters per second squared).
7. **r** is the radius of the capillary tube or pore (in meters).

1.12 Contact Angle of fluid

The contact angle of a fluid refers to the angle formed between the tangent line of the liquid-vapor interface and the solid surface at the point of contact. It is a measurement that characterizes the wetting behavior of a fluid on a solid substrate [53]. Measuring and understanding a fluid's contact angle on a solid surface provides important insights into wetting behavior, surface interactions, and the design of materials with specific surface properties.

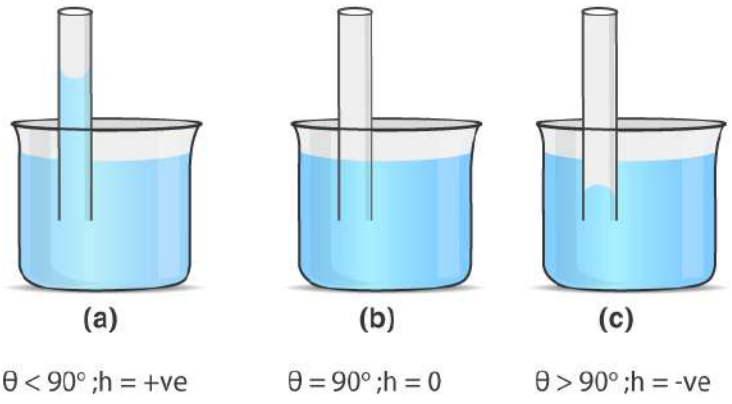

Figure 1.5: Different contact angles of water [56]

1.13 Surface Tension of fluid

The cohesive forces between molecules at the liquid's surface are referred to as surface tension. It is the amount of energy necessary to raise the liquid's surface area. The molecules in the liquid's bulk are subjected to attractive forces from neighboring molecules in all directions. However, because the molecules near the surface have fewer neighboring molecules above them, the forces acting on them are imbalanced. This imbalance causes the creation of a thin, elastic-like layer at the liquid's surface, which operates as if it were under strain. The surface tension is seen in this stratum.

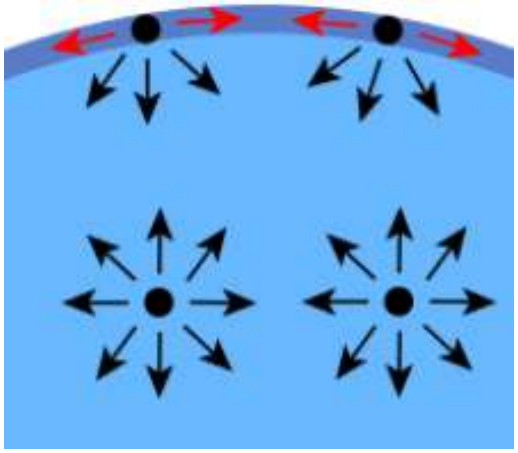

Figure 1.6: Concept of surface tension [57]

Surface tension is the ratio of surface force induced by liquid pressure to the length along which the forces act. It can be expressed as

$$T = \frac{F}{L} \tag{1.6}$$

T = Surface tension of liquid

F = Surface force acting per unit length

L = Length on which force

References

[1] F. Boukid, "Smart Food Packaging: An Umbrella Review of Scientific Publications," *Coatings*, vol. 12, no. 12, p. 1949, Dec. 2022, doi: 10.3390/coatings12121949.

[2] D. Schaefer and W. M. Cheung, "Smart Packaging: Opportunities and Challenges," *Procedia CIRP*, vol. 72, pp. 1022–1027, 2018, doi: 10.1016/j.procir.2018.03.240.

[3] H. Cheng *et al.*, "Recent advances in intelligent food packaging materials: Principles, preparation and applications," *Food Chem*, vol. 375, p. 131738, May 2022, doi: 10.1016/j.foodchem.2021.131738.

[4] P. Taoukis, "Use of time–temperature integrators and predictive modelling for shelf life control of chilled fish under dynamic storage conditions," *Int J Food Microbiol*, vol. 53, no. 1, pp. 21–31, Dec. 1999, doi: 10.1016/S0168-1605(99)00142-7.

[5] A. Pavelková, "Time temperature indicators as devices intelligent packaging," *Acta Universitatis Agriculturae et Silviculturae Mendelianae Brunensis*, vol. 61, no. 1, pp. 245–251, Apr. 2013, doi: 10.11118/actaun201361010245.

[6] J. D. Selman, "Time—temperature indicators," in *Active Food Packaging*, Boston, MA: Springer US, 1995, pp. 215–237. doi: 10.1007/978-1-4615-2175-4_10.

[7] D. Georgiou, E. P. Kalogianni, G. Dimitreli, E. Ftouli, and S. Parisi, "Capillary penetration for the development of a method for the assessment of shelf-life of foods," *Journal of Food Measurement and Characterization*, vol. 17, no. 2, pp. 1167–1174, Apr. 2023, doi: 10.1007/S11694-022-01685-8/FIGURES/9.

[8] "Novel Food Packaging Techniques - Google Books." https://books.google.com.pk/books?hl=en&lr=&id=6RWkAgAAQBAJ&oi=fnd&pg=PA103&dq=applications+of+time+temperature+indicator&ots=NPL2R_OEyh&sig=9VHqqcTzCdyegL6DEwB1nlpMQjA&redir_esc=y#v=onepage&q=applications%20of%20time%20temperature%20indicator&f=false (accessed Jun. 11, 2023).

[9] A. K. Yetisen, M. S. Akram, and C. R. Lowe, “Paper-based microfluidic point-of-care diagnostic devices,” *Lab Chip*, vol. 13, no. 12, p. 2210, 2013, doi: 10.1039/c3lc50169h.

[10] W. Dungchai, O. Chailapakul, and C. S. Henry, “A low-cost, simple, and rapid fabrication method for paper-based microfluidics using wax screen-printing,” *Analyst*, vol. 136, no. 1, pp. 77–82, 2011, doi: 10.1039/C0AN00406E.

[11] A. W. Martinez, S. T. Phillips, M. J. Butte, and G. M. Whitesides, “Patterned Paper as a Platform for Inexpensive, Low-Volume, Portable Bioassays,” *Angewandte Chemie International Edition*, vol. 46, no. 8, pp. 1318–1320, Feb. 2007, doi: 10.1002/anie.200603817.

[12] Y. Yang, E. Noviana, M. P. Nguyen, B. J. Geiss, D. S. Dandy, and C. S. Henry, “Paper-Based Microfluidic Devices: Emerging Themes and Applications,” *Anal Chem*, vol. 89, no. 1, pp. 71–91, Jan. 2017, doi: 10.1021/acs.analchem.6b04581.

[13] L. Sun *et al.*, “A novel, simple and low-cost paper-based analytical device for colorimetric detection of Cronobacter spp.,” *Anal Chim Acta*, vol. 1036, pp. 80–88, Dec. 2018, doi: 10.1016/j.aca.2018.05.061.

[14] X. Li, J. Tian, T. Nguyen, and W. Shen, “Paper-Based Microfluidic Devices by Plasma Treatment,” *Anal Chem*, vol. 80, no. 23, pp. 9131–9134, Dec. 2008, doi: 10.1021/ac801729t.

[15] J. Banks, J. Watt, J. Banks, and J. Watt, “On a New Method of Preparing a Test Liquor to Shew the Presence of Acids and Alkalies in Chemical Mixtures. By Mr. James Watt, Engineer; Communicated by Sir Joseph Banks, Bart. P. R. S.,” *RSPT*, vol. 74, pp. 419–422, 1784, Accessed: Jun. 11, 2023. [Online]. Available: https://ui.adsabs.harvard.edu/abs/1784RSPT...74..419B/abstract

[16] J. P. Comer, “Semiquantitative Specific Test Paper for Glucose in Urine,” *Anal Chem*, vol. 28, no. 11, pp. 1748–1750, Nov. 1956, doi: 10.1021/ac60119a030.

[17] G. Toennies and J. J. Kolb, “Techniques and Reagents for Paper Chromatography,” *Anal Chem*, vol. 23, no. 6, pp. 823–826, Jun. 1951, doi: 10.1021/AC60054A002/ASSET/AC60054A002.FP.PNG_V03.

[18] J. H. W. Leuvering, P. J. H. M. Thal, M. van der Waart, and A. H. W. M. Schuurs, “Sol Particle Immunoassay (SPIA),” *J Immunoassay*, vol. 1, no. 1, pp. 77–91, Jan. 1980, doi: 10.1080/01971528008055777.

[19] H. Asano and Y. Shiraishi, “Development of paper-based microfluidic analytical device for iron assay using photomask printed with 3D printer for fabrication of hydrophilic and hydrophobic zones on paper by photolithography,” *Anal Chim Acta*, vol. 883, pp. 55–60, Jul. 2015, doi: 10.1016/j.aca.2015.04.014.

[20] X. Li, J. Tian, T. Nguyen, and W. Shen, “Paper-Based Microfluidic Devices by Plasma Treatment,” *Anal Chem*, vol. 80, no. 23, pp. 9131–9134, Dec. 2008, doi: 10.1021/ac801729t.

[21] E. Carrilho, A. W. Martinez, and G. M. Whitesides, “Understanding Wax Printing: A Simple Micropatterning Process for Paper-Based Microfluidics,” *Anal Chem*, vol. 81, no. 16, pp. 7091–7095, Aug. 2009, doi: 10.1021/ac901071p.

[22] J. Nie *et al.*, “Low-Cost Fabrication of Paper-Based Microfluidic Devices by One-Step Plotting,” *Anal Chem*, vol. 84, no. 15, pp. 6331–6335, Aug. 2012, doi: 10.1021/ac203496c.

[23] T. Songjaroen, W. Dungchai, O. Chailapakul, and W. Laiwattanapaisal, “Novel, simple and low-cost alternative method for fabrication of paper-based microfluidics by wax dipping,” *Talanta*, vol. 85, no. 5, pp. 2587–2593, Oct. 2011, doi: 10.1016/j.talanta.2011.08.024.

[24] K. Maejima, S. Tomikawa, K. Suzuki, and D. Citterio, “Inkjet printing: an integrated and green chemical approach to microfluidic paper-based analytical devices,” *RSC Adv*, vol. 3, no. 24, p. 9258, 2013, doi: 10.1039/c3ra40828k.

[25] J. Olkkonen, K. Lehtinen, and T. Erho, "Flexographically Printed Fluidic Structures in Paper," *Anal Chem*, vol. 82, no. 24, pp. 10246–10250, Dec. 2010, doi: 10.1021/ac1027066.

[26] G. Chitnis, Z. Ding, C.-L. Chang, C. A. Savran, and B. Ziaie, "Laser-treated hydrophobic paper: an inexpensive microfluidic platform," *Lab Chip*, vol. 11, no. 6, p. 1161, 2011, doi: 10.1039/c0lc00512f.

[27] V. F. Curto, N. Lopez-Ruiz, L. F. Capitan-Vallvey, A. J. Palma, F. Benito-Lopez, and D. Diamond, "Fast prototyping of paper-based microfluidic devices by contact stamping using indelible ink," *RSC Adv*, vol. 3, no. 41, p. 18811, 2013, doi: 10.1039/c3ra43825b.

[28] S. A. Klasner, A. K. Price, K. W. Hoeman, R. S. Wilson, K. J. Bell, and C. T. Culbertson, "Paper-based microfluidic devices for analysis of clinically relevant analytes present in urine and saliva," *Anal Bioanal Chem*, vol. 397, no. 5, pp. 1821–1829, Jul. 2010, doi: 10.1007/s00216-010-3718-4.

[29] A. C. Glavan *et al.*, "Rapid fabrication of pressure-driven open-channel microfluidic devices in omniphobic RF paper," *Lab Chip*, vol. 13, no. 15, p. 2922, 2013, doi: 10.1039/c3lc50371b.

[30] P. D. Haller, C. A. Flowers, and M. Gupta, "Three-dimensional patterning of porous materials using vapor phase polymerization," *Soft Matter*, vol. 7, no. 6, p. 2428, 2011, doi: 10.1039/c0sm01214a.

[31] Md. A. Mahmud, E. J. M. Blondeel, M. Kaddoura, and B. D. MacDonald, "Creating compact and microscale features in paper-based devices by laser cutting," *Analyst*, vol. 141, no. 23, pp. 6449–6454, 2016, doi: 10.1039/C6AN02208A.

[32] M. M. Thuo *et al.*, "Fabrication of Low-Cost Paper-Based Microfluidic Devices by Embossing or Cut-and-Stack Methods," *Chem. Mater*, vol. 26, no. 14, pp. 4230–4237, 2014, doi: 10.1021/cm501596s.

[33] J. Nie, Y. Liang, Y. Zhang, S. Le, D. Li, and S. Zhang, “One-step patterning of hollow microstructures in paper by laser cutting to create microfluidic analytical devices,” *Analyst*, vol. 138, no. 2, pp. 671–676, 2013, doi: 10.1039/C2AN36219H.

[34] E. M. Fenton, M. R. Mascarenas, G. P. López, and S. S. Sibbett, “Multiplex Lateral-Flow Test Strips Fabricated by Two-Dimensional Shaping,” *ACS Appl Mater Interfaces*, vol. 1, no. 1, pp. 124–129, Jan. 2009, doi: 10.1021/am800043z.

[35] Y. S. Kim, Y. Yang, and C. S. Henry, “Laminated and infused Parafilm® – paper for paper-based analytical devices,” *Sens Actuators B Chem*, vol. 255, pp. 3654–3661, Feb. 2018, doi: 10.1016/j.snb.2017.10.005.

[36] T. Ozer, C. McMahon, and C. S. Henry, “Advances in Paper-Based Analytical Devices,” *https://doi.org/10.1146/annurev-anchem-061318-114845*, vol. 13, pp. 85–109, Jun. 2020, doi: 10.1146/ANNUREV-ANCHEM-061318-114845.

[37] J. Noiphung, K. Talalak, I. Hongwarittorrn, N. Pupinyo, P. Thirabowonkitphithan, and W. Laiwattanapaisal, “A novel paper-based assay for the simultaneous determination of Rh typing and forward and reverse ABO blood groups,” *Biosens Bioelectron*, vol. 67, pp. 485–489, May 2015, doi: 10.1016/j.bios.2014.09.011.

[38] M. Al-Tamimi, W. Shen, R. Zeineddine, H. Tran, and G. Garnier, “Validation of Paper-Based Assay for Rapid Blood Typing,” *Anal Chem*, vol. 84, no. 3, pp. 1661–1668, Feb. 2012, doi: 10.1021/ac202948t.

[39] N. A. Meredith, C. Quinn, D. M. Cate, T. H. Reilly, J. Volckens, and C. S. Henry, “Paper-based analytical devices for environmental analysis,” *Analyst*, vol. 141, no. 6, pp. 1874–1887, 2016, doi: 10.1039/C5AN02572A.

[40] Y. F. Sasaki *et al.*, “The comet assay with 8 mouse organs: results with 39 currently used food additives,” *Mutation Research/Genetic Toxicology and Environmental Mutagenesis*, vol. 519, no. 1–2, pp. 103–119, Aug. 2002, doi: 10.1016/S1383-5718(02)00128-6.

[41] L. Busa, S. Mohammadi, M. Maeki, A. Ishida, H. Tani, and M. Tokeshi, “Advances in Microfluidic Paper-Based Analytical Devices for Food and Water Analysis,” *Micromachines (Basel)*, vol. 7, no. 5, p. 86, May 2016, doi: 10.3390/mi7050086.

[42] G. Fancher, “Henry Darcy - Engineer and Benefactor of Mankind,” *Journal of Petroleum Technology*, vol. 8, no. 10, pp. 12–14, Oct. 1956, doi: 10.2118/762-G.

[43] S. Friedlander, “Stability of Flows,” in *Encyclopedia of Mathematical Physics*, Elsevier, 2006, pp. 1–7. doi: 10.1016/B0-12-512666-2/00252-2.

[44] G. O. Brown, “Henry Darcy and the making of a law,” *Water Resour Res*, vol. 38, no. 7, pp. 11-1-11–12, Jul. 2002, doi: 10.1029/2001WR000727.

[45] “Morris Muskat - Wikipedia.” https://en.wikipedia.org/wiki/Morris_Muskat (accessed Jun. 11, 2023).

[46] S. G. ADVANI and E. M. SOZER, “Liquid Molding of Thermoset Composites,” *Comprehensive Composite Materials*, pp. 807–844, 2000, doi: 10.1016/B0-08-042993-9/00171-6.

[47] “Introduction to Modeling of Transport Phenomena in Porous Media - Jacob Bear, Y. Bachmat - Google Books.” https://books.google.com.pk/books?id=MOaoeI9aAc0C&printsec=frontcover&source=gbs_ge_summary_r&cad=0#v=onepage&q&f=false (accessed Jun. 11, 2023).

[48] “What is Viscosity ? States Newton’s Law of Viscosity & define Newtonian and Non-Newtonian fluid – Mechanical Engineering.” https://mechaengineerings.wordpress.com/2015/05/25/viscosity/ (accessed Jun. 11, 2023).

[49] “Rheology - Volume I - Google Books.” https://books.google.com.pk/books?hl=en&lr=&id=zjw7CwAAQBAJ&oi=fnd&pg=PA74&dq=newton%27s+law+of+viscosity&ots=huwAXqU1i5&sig=izgpiGRuEhMlp8HmzNa9hWGw8TY&redir_esc=y#v=onepage&q=newton’s%20law%20of%20viscosity&f=false (accessed Jun. 11, 2023).

[50] “Richard E. Lucas’s research works | Michigan State University, MI (MSU) and other places.” https://www.researchgate.net/scientific-contributions/Richard-E-Lucas-39535334 (accessed Jun. 11, 2023).

[51] K. Li, D. Zhang, H. Bian, C. Meng, and Y. Yang, “Criteria for Applying the Lucas-Washburn Law,” *Scientific Reports 2015 5:1*, vol. 5, no. 1, pp. 1–7, Sep. 2015, doi: 10.1038/srep14085.

[52] “Capillary Zone - an overview | ScienceDirect Topics.” https://www.sciencedirect.com/topics/earth-and-planetary-sciences/capillary-zone (accessed Jun. 11, 2023).

[53] P.-G. de Gennes, F. Brochard-Wyart, and D. Quéré, “Capillarity and Wetting Phenomena,” *Capillarity and Wetting Phenomena*, 2004, doi: 10.1007/978-0-387-21656-0.

[54] H.-J. Butt, K. Graf, and M. Kappl, “Contact Angle Phenomena and Wetting,” *Physics and Chemistry of Interfaces*, pp. 118–144, Aug. 2004, doi: 10.1002/3527602313.CH7.

[55] “Pinterest.” https://www.pinterest.com/pin/546202261050533016/ (accessed Jun. 11, 2023).

[56] “Capillary Action - Meaning, Definition, Examples, Adhesion, Cohesion.” https://byjus.com/jee/capillary-action/ (accessed Jun. 11, 2023).

[57] “Surface Tension: Definition, Examples, Applications of Surface Tension.” https://www.toppr.com/guides/physics/properties-of-fluids/surface-tension/ (accessed Jun. 11, 2023).

[58] Y. S. Kim, Y. Yang, and C. S. Henry, “Laminated and infused Parafilm® - paper for paper-based analytical devices,” *Sens Actuators B Chem*, vol. 255, no. 3, pp. 3654–3661, Feb. 2018, doi: 10.1016/J.SNB.2017.10.005.

Chapter 2

Flow control in porous media by cavities using numerical and experimental approach

(Contents of this Chapter will be submitted to International Journal)

Abstract

This research explores the flow in porous media by the virtue of capillary penetration and ways of controlling the liquid imbibition rate. We conduct experiments and simulations to alter the flow resistance either by varying the liquids and/or changing the paper channel geometry by adding cavities. A simulation model was developed to compare the numerical results with experiments. Both experiments and simulations were conducted on a porous media in the form of lateral strips of dimensions ($\ell \times w$) = (12 × 2) cm cut out from Whatman grade-42 filter paper. Capillary penetration rate with three different liquids, i.e., water, olive oil, and castor oil, was measured and extensive experimental data is presented. From experiments, it was revealed that by creating a circular cavity in the paper channel, penetration rate was sufficiently altered. Moreover, increasing the cavities size and type of liquid (w.r.t. viscosity) also caused a decrease in the flow rate. Liquid imbibition rates were also influenced by the position of the cavities in the paper channel. Cavities placed near the lower edge of the strip decreased the liquid imbibition rate much more by offering more flow resistance than those placed further away. A good agreement was observed with results obtained from both experimental and numerical approaches. We believe that this research would help in developing advance techniques to enhance the flow control strategies in microfluidic paper-based analytical devices (μPADs) and indicators that have a wide range of applications in various areas of science and technology including food quality management, medical diagnostics, and environmental monitoring.

Keywords: Porous media, Flow control, Channel cavity, μPADs, Experiments, and simulation

2.1 Introduction

With ever growing world population, new challenges such as global health issues including food security and the diagnosis/prevention of new diseases have become even more important in today's world. Every year, over 1.3 billion tons of edible food are wasted or lost during the food supply process as a result of no check on its quality or hygiene [1]. Food security has become even more essential as a result of the recent new epidemic. Against this backdrop, it is imperative to monitor the quality of food [3]. One of the remedies could be to check and monitor the factors upon which the quality of the perishable food items is dependent such as time span of food supply chain and/or environmental conditions including temperature, and humidity [2]. Waste intelligent packaging with condition monitoring indicators during travel and storage can also serve the purpose [3], [4]. These devices/indicators also play an effective role in determining the remaining shelf life of perishable products [5], [6] and serve as of quality sensors for the safety of food in order to minimize waste [5].

Microfluidics deals with the study of the manipulation and the control of micro/nano liters of fluid flow on small scale. They provide promising means of developing devices for monitoring and diagnostic applications. Since 21st century, there is an advent in studies related to paper-based microfluidics devices due to its easy fabrication, simpler construction, lower cost, and no maintenance cost [7]. One of the advantages of these devices is the use of porous paper as a substrate that can facilitate the fluid flow through it by capillary forces [8], [9]. Microfluidic paper-based analytical devices (μPADs) are capable of medical diagnostics [10] – [12] food quality control [3], [4], [6], [13], [14] as well as environmental monitoring [15], [16]. Moreover, for many years, study on fluid flow through porous media has been a priority, particularly in the areas of groundwater movement, petroleum engineering, geology, and geophysics. Knowledge of flow control in paper-based microfluidic devices is essential for the accuracy of the device [17], [18]. The main principle used in these devices is simple fluid imbibition, which is a type of capillary flow in porous media. Capillary action is the ability of a liquid to flow through channels as a result of surface tension [19]. Previously, Lucas (1918) and Washburn et al. (1921) deduced the relationship between the liquid imbibition distance and the time for

capillary in tubes, it is referred to as the Lucas-Washburn equation. The work of Lucas and Washburn helped to understand the capillary flow in porous media [20], [21]. The Lucas Washburn equation $L^2 = \frac{\gamma r t \cos(\theta)}{2\mu}$ (where L is the rise of fluid in capillary, θ is the contact angle of fluid, γ is the surface tension, μ is the dynamic viscosity, r is the radius of capillary tube, and *t* is the time period of imbibition) and the Boussinesq equation [22] $\frac{\partial}{\partial t} w(x,t) = \frac{\partial}{\partial x}\left(w(x,t)\frac{\partial}{\partial x} w(x,t)\right)$ where (x,t) is a non-negative scalar function on the interval (0,1) and time $t \in \mathbb{R} > 0$ can both be used to describe the fluid model in porous media. This is dependent on fluid characteristics such as density and viscosity, and the characteristics of porous media such as porosity, pore size, and permeability. Additionally, the fluid's molecular make-up, pressure, and temperature affect its density and viscosity. There are different methods to control the flow rate in the paper that is required for better resolution in μPADs. The rate of capillary penetration mostly depends on the liquids and properties of porous medium. There are three categories of flow control strategies: geometric, chemical, and mechanical [23], [24]. Geometry-based techniques depend on differences in channel length, channel width, and obstructions in the flow path that may cause the fluid to take longer to reach the detecting zone. Gravity, capillary absorption, and viscous forces all contribute to fluid flow in porous media. Depending on the needs of the study, fluid flow can be represented using radial geometry, 1D, 2D, or 3D visualization [25], [26]. A small change in the rate of fluid flow can lead to erroneous results in these devices. Despite advances in paper technology, fluid flow control still remains challenging due to inherent vulnerabilities and variabilities in the paper material and the passive nature of flow by capillary action through the pores. To the best of our knowledge, we found no work on the physical control of fluid flow by the creation of cavities in the main paper channel.

In this work, the variables that affect the rate of capillary penetration in porous media are studied using simulation and experiments. Whatman grade 42 paper and liquids (water, olive oil, and castor oil) with different physical properties are selected. Experiments are performed by altering the geometry of porous media, i.e., creating circular cavities of different sizes at different positions of the paper channel. A simulation model of wicking in porous media is developed, and the experimental results are compared. With an increase

in flow resistance by the virtue of channel cavities, a time delay in fluid flow occurs. Therefore, a new method for flow control is presented.

2.2 Materials and methods

2.2.1 Experimental Method

For performing experiments on porous media strips, Whatman Grade 42 filter papers (1442-042 Ashless Filter Paper) are used, with properties as shown in **Table 1.**

Table 1: Properties of Porous Matrix Whatman paper

Paper Grade	Particle Retention Liquid (µm)	Filtration Speed Herzberg (s)	Typical thickness (µm)	Basis Weight (g/m^3)
42	0.25	1870	200	100

Three different liquids, i.e., mineral water (Nestle, Pakistan), olive oil (Himani, Pakistan), and castor oil (Mundial, Pakistan), are used for fluid imbibition. The detailed liquid properties are given in **Table 2.**

Table 2: Properties of Fluids.

Sr. #.	Fluid	Density (kg/m^3)	Viscosity (Pa.s)	Porosity	Surface Tension	Permeability m^3
1.	Water	997	0.001	0.199	0.0732	3.886×10^{-16}
2.	Olive oil	917	0.084	0.165	0.032	3.227×10^{-16}
3.	Castor oil	961	0.58	0.182	0.039	3.557×10^{-16}
4.	Air	1	1.76×10^{-5}	N/A	N/A	N/A

A petri dish is used as a liquid reservoir. To cut out the paper with exactitude in order to create lateral strips of dimensions ($\ell \times w$) = (12 × 2) cm, a paper cutter machine (Guillotine, Pakistan) is used, which ensures that each sheet is uniform and consistent. After cutting

filter paper strips, cavities of different diameters, such as 16 mm, 12 mm, and 8 mm, were created using a die. For each experiment, strips were held by a sturdy stand with one strip edge dipped in the reservoir. A camera (Nikon Full HD 1080 pixels) with a micro lens (DMWIFI) was connected to a computer and videos of the fluid imbibition through the entire length of the strip were recorded. Recorded videos were post-processed for data acquisition after every 1 cm rise of fluid in the paper strip. Experiments were performed both for a simple strip with no cavity and for strips with cavities using all three liquids. To ensure the accuracy and reliability of the results, each experiment was performed at least three times. A schematic of strip fabrication and experimental setup is as shown in **Figure 2.1 (a).** For measuring the paper porosity, a high-precision weight balance was used to measure the paper mass. Mass of dry paper and mass after liquid imbibition in porous media were measured, and then porosity (ϕ) was measured by the formula, ϕ = void volume/ total volume, as shown in **Figure 2.1 (b).** For instance, the weight of a dry paper strip was measured as 0.23 g and that of a wet paper strip with mineral water, olive oil and castor oil were 0.39 g, 0.35 g and 0.37 g, respectively. The corresponding porosity values were calculated as 0.199, 0.165, and 0.182, respectively.

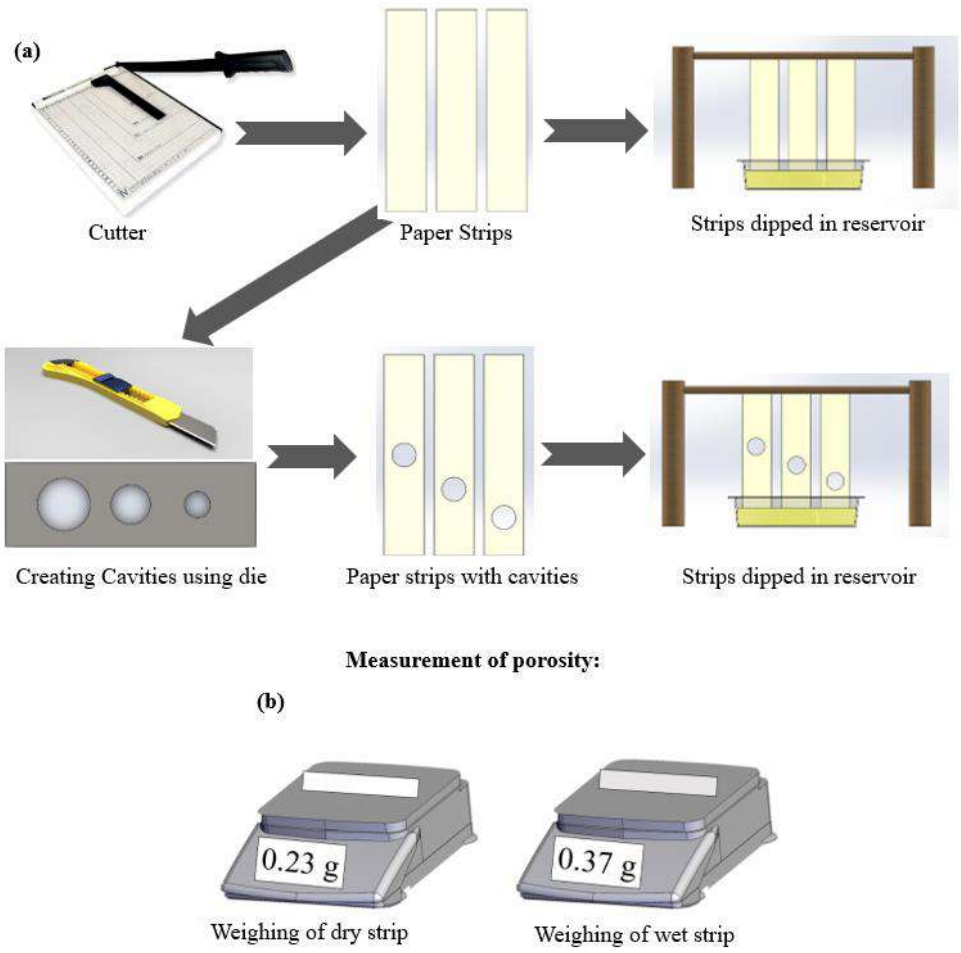

Figure 2.1: (a) Fabrication of paper strips using paper cutter and experimental setup **(b)** Measurement of weight of dry and imbibed paper strips using weight balance.

2.2.2 Simulation Model

A simulation model was developed using laminar flow and phase transport in porous media formulations. The formulations were implemented using COMSOL Multiphysics 5.6. The numerical domain of 2 cm width and 12 cm length with boundary conditions was used as shown in **Figure 2.2 (a).** A paper thickness of 0.2 mm and pore radius of 0.25 µm were considered throughout the simulations unless stated explicitly. Different parameters such as porosity, density, viscosity, surface tension, cavity size, and location were varied. In phase transfer physics, we assumed that there was some amount of air trapped in the pores of the dry strip that escapes only from the upper boundary designated as 3 in order to fill the pores with fluid, and we insulated the remaining boundaries. At this boundary, we

applied mass flux $\frac{\text{P\_lm}}{\text{th}}[\frac{\text{kg}}{\text{m.s}}]$ for the air phase, which results from the pressure gradient given in the Darcy model. Here, p_lm is the Lagrange multiplier representative of flux at the boundary. It was introduced as an additional variable to solve when the weak constraints were turned on for this boundary in the Darcy's law interface. As the Lagrange multiplier does not take the thickness (th) of the paper strip into account, the flux must be divided by it. We also defined the effect of gravity on porous media.

Darcy's law was used to achieve the pressure gradient for fluid flow through the porous media. So, for the boundary designated as 1, the boundary condition was the hydrostatic atmospheric pressure (P_{atm}) for the water phase, and for the boundary designated as 3, the boundary condition was the hydrostatic atmospheric pressure (P_{atm}) minus the capillary pressure (P_c). We assumed that the remaining two side boundaries (2 and 4) would not affect the flow as there is no mass flux entering or leaving, so consider it insulated.

2.2.3 Meshing

After creating geometry and assigning multi-physics to our model, next step was to build the mesh. Mesh plays an important role to solve the model by dividing geometry into very small elements and solving a finite element problem. It regulates factors such as: size, shape, density, and number of elements in the geometry.

The linear distributive mesh was erected for our model using mapped mesh tool as liquid imbibing through porous media is a linear function. We had chosen normal mesh for simulation as the simulation results for fine mesh and normal mesh were very close as established by the grid independency test. Our mesh size contained maximum and minimum element size, growth rate, correction factor and resolution of narrow edges of 0.00804 and 3.6E-5, 1.3, 0.3 and 1, respectively. Additionally, it also reduced the computational cost and the time of study. The mesh generated for our model is shown in **Figure 2.2 (b).**

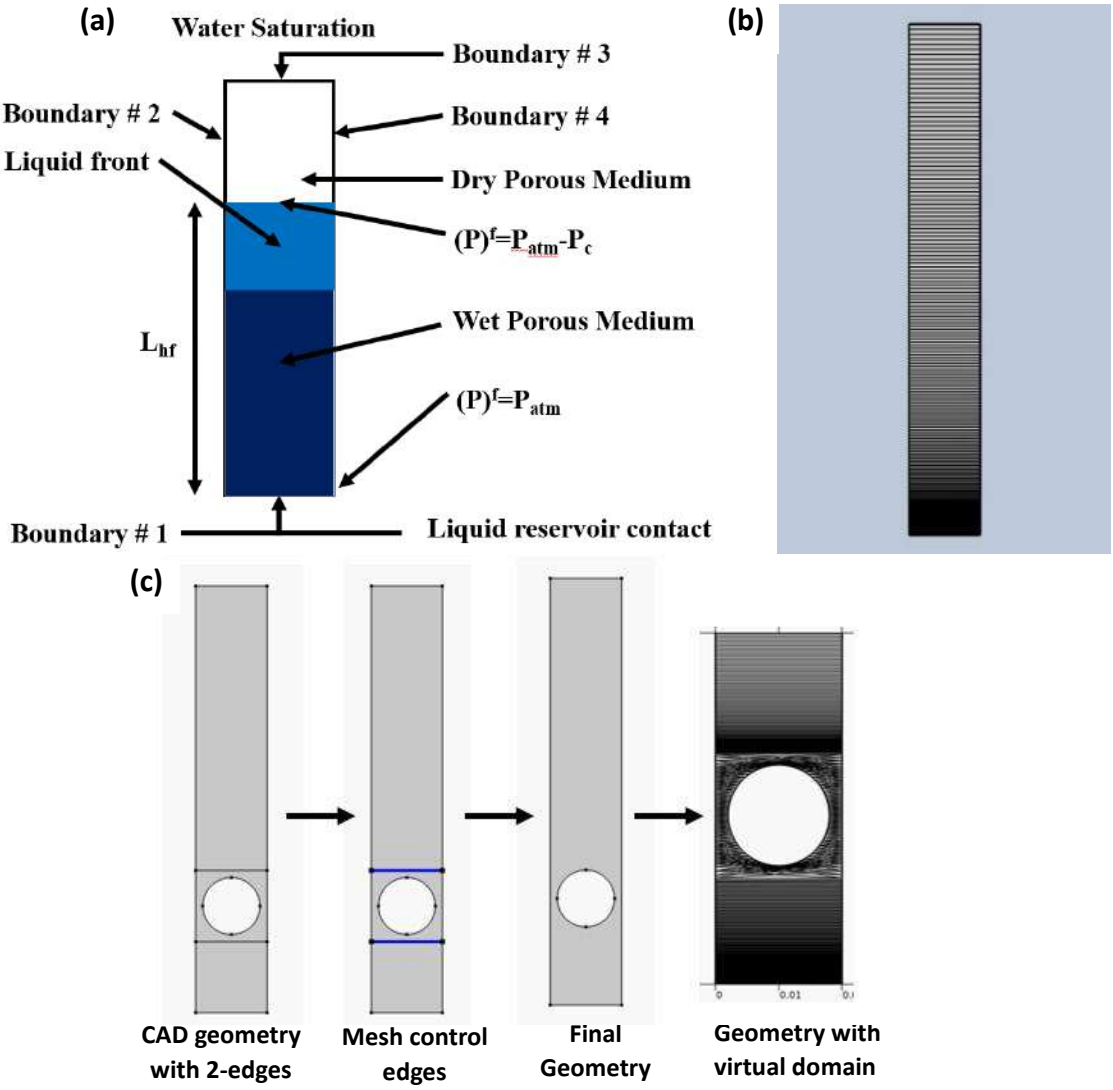

Figure 2.2: (a) Numerical domain with boundary conditions, **(b)** Meshing of numerical domain without cavity**,** and **(c)** Meshing of numerical domain with cavity using virtual operations.

In our simulation analysis, for studying cavity ridden paper channel**,** we used virtual operations to define the virtual rectangular domain and the mesh control edges around the cavity and created a triangular mesh in the region. This facilitated the formation of mesh with different types and sizes within a single domain. Mesh size for the domain with or without cavity ware kept the same.

2.2.4 Governing Equation

The simulation is based on Multiphase flow in porous media which fully couples Darcy's Law and phase transport in porous media. Phase transport in porous media uses the equation given below for the volumetric fraction s'_f of wetting and nonwetting fluid f.

$$\frac{\delta}{\delta t}\left(\varepsilon_p \rho_f s'_f\right) + \nabla \cdot \left(-\rho_f K \frac{K_{rf}}{\mu_f}\left(\nabla P_f - \rho_f g\right)\right) = Q_f = 0 \quad \textbf{(2.1)}$$

where $\boldsymbol{\varepsilon_p}$ is the porosity of the media, $\boldsymbol{\rho_f}$ is the fluid density (kg/m^3), $\boldsymbol{s'_f}$ is the volumetric fraction, **K** is the permeability (m^2), $\mathbf{K_{rf}}$ is the relative permeability, $\boldsymbol{\mu_f}$ is the dynamic viscosity (Ns/m^2), $\mathbf{P_f}$ is the pressure (Pa), and **g** is the gravity.

As the total of wetted s'_2 and nonwetted s'_1volume fractions of the two phases are 1, the residual volume fraction is calculated from.

$$s'_1 = 1 - s'_2 \quad \textbf{(2.2)}$$

The calculation of capillary pressure P_C depends on the saturation of the wetting phase s'_w, also known as s'_2 in the model, and the entry capillary pressure P_{ecp}. The Brooks and Corey model is utilized to determine the capillary pressure.

$$P_C = P_{ecp} \frac{1}{(\overline{s'_w})^{\frac{1}{\lambda}}} \quad \textbf{(2.3)}$$

$$K_{rs'_w} = (\overline{s'_w})^{(3+\frac{2}{\lambda})} \quad \textbf{(2.4)}$$

$$K_{rs'_n} = (\overline{s'_n})^2(1 - (1 - \overline{s'_n})^{(1+\frac{2}{\lambda})} \quad \textbf{(2.5)}$$

where λ is the pore distribution index, $K_{rs'_w}$is the relative permeabilities wetting phases, and $K_{rs'_n}$is the relative permeabilities nonwetting phases.

The Darcy's law formulations are a combination of Darcy's law and the continuity equation. This interface is used to describe the flow of a fluid through a permeable medium, such as porous paper, rock, or soil. By combining these two equations, Darcy's Law interface can provide a more accurate description of fluid flow in porous media.

$$\frac{\delta}{\delta t}\left(\rho\varepsilon_p\right) + \nabla \cdot \rho\left(-\frac{K}{\mu}(\nabla P)\right) = 0 \quad \textbf{(2.6)}$$

The Lucas-Washburn equation was used to calculate the length of fluid imbibition in porous or capillary media as a function of diffusion co-efficient and wicking time.

According to the Lucas-Washburn Equation, "the rise of fluid in a capillary is proportional to the square root of the capillary's radius, time taken for wicking, and fluid parameters, such as contact angle and surface tension, and inversely related to dynamic viscosity of fluid."

$$L^2 = \frac{\gamma r t\, cos(\theta)}{2\mu} \quad \textbf{(2.7)}$$

where L is the rise of fluid in capillary, θ is the contact angle of fluid, γ is the surface tension of fluid, μ is the dynamic viscosity, *r* is the radius of capillary tube, and *t* is the time period of imbibition.

2.3 Validation of Numerical Technique

The simulation model was validated against the experiments and Lucas Washburn (L-W) equation (eq. 2.7) of fluid flow. Experiments were performed for water imbibition in porous media. **Figure 2.3 (a)** shows that the results obtained by simulations are in a good agreement with those obtained by experiments and Lucas-Washburn equation. **Figure 2.3 (b)** shows the water saturation at successive time intervals obtained from simulation.

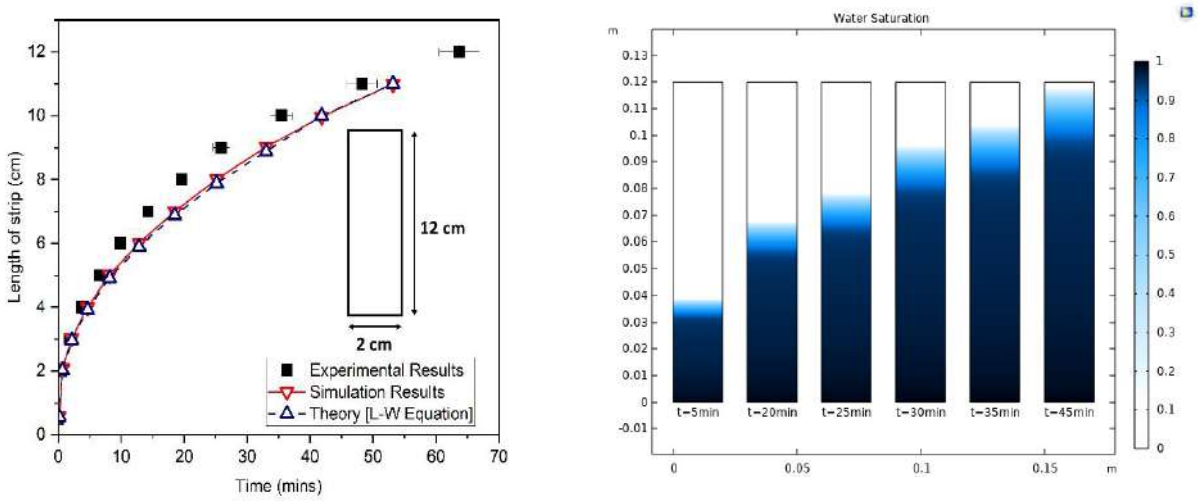

Figure 2.3: (a) Validation of simulation model against experiment and theoretical Lucas Washburn (L-W) equation (eqn. 2.7), **(b)** Simulation results. Water is used as an imbibing liquid.

2.4 Results and Discussions

The basic aim of this research is to develop effective methods to reduce the flow rate in porous media. Here, we explore different means of flow control such as the use of cavities of different sizes at different locations under various set of conditions using experimental and numerical approaches. Flux variations of different fluids such as water, olive oil and castor oil are studied through lateral strips fabricated from Whatman 42 filter paper.

Firstly, we perform our experiments on paper strip of length 12 cm and width 2 cm. **Figure 2.4 (a)** shows the liquid ambition with time along the strip length using different liquids. Results show that as we use higher viscosity fluids flow rate decreases i.e., requires more time to travel. **Figure 2.4 (b)** shows simulation results comparison at same time for different liquids. There is a prominent difference between water saturation, olive oil

saturation and castor oil saturation. At t = 50 mins water saturation is almost complete whereas olive oil saturation reached above at 2 cm along the length of strip and castor oil saturation almost reached 1 cm along the length of strip. This indicates that castor oil imbibition is almost 10 times slower than water.

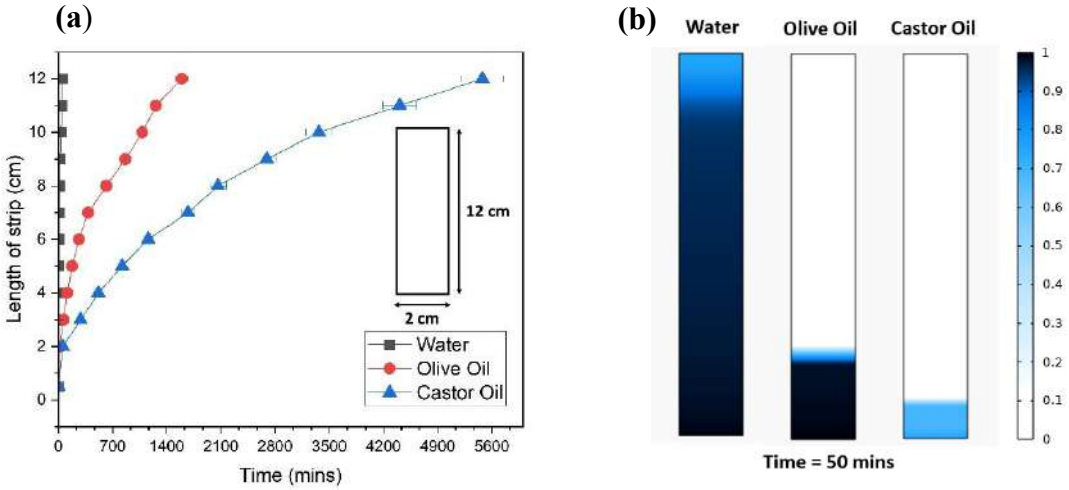

Figure 2.4: (a) Experimental results of liquid imbibition with time along the strip length without cavity using different liquids, **(b)** Comparison of simulation results using different liquids at same time.

2.4.1 Effect of Circular Cavities

Figure 2.5 shows the simulation results comparison at same time for different liquids with circular cavity of diameter 16 mm located at 3 cm from the strip edge. The flow rate has decreased and the water saturation at t = 70 mins is only up to 8 cm of the strip. Similarly, the olive and castor oil imbibition has reduced with the inclusion of cavities in the water flow channel water.

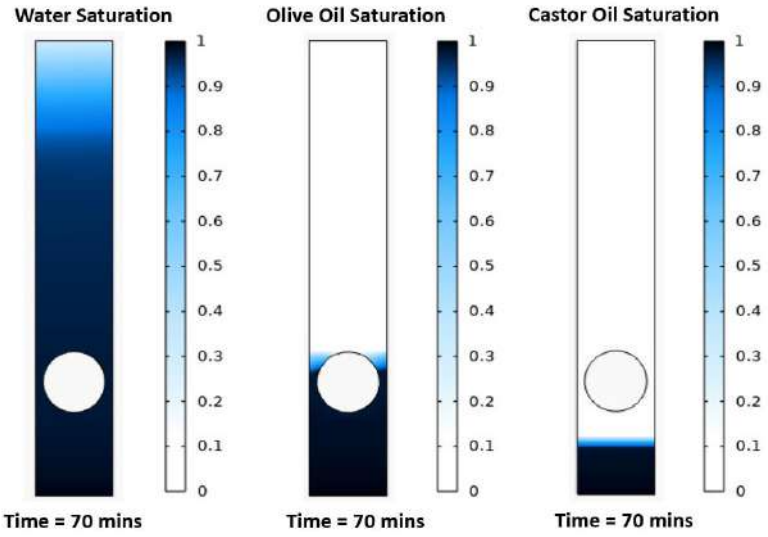

Figure 2.5: Simulation results of liquid imbibition with time along the strip length with cavity of 16 mm diameter using different liquids.

Further, we added circular cavities of diameter 8 mm, 12 mm, and 16 mm to check the effect on fluid imbibition in porous media. **Figure 2.6** shows comparison of simulation and experimental results of liquid imbibition with time along the strip with circular cavity at 6 cm from strip edge using different liquids. In **Figure 2.6 (a),** we created circular cavity of 8 mm at 6 cm from strip edge and water is used as a fluid. Result shows the 19.5% decrease in flow rate as compared to strips without cavity. In **Figure 2.6 (b),** we created circular cavity of 12 mm at 6 cm from strip edge and water is used as fluid. Result shows the 37.4% and 15% decrease in flow rate as compared to strips without cavity and with cavity of 8 mm respectively. In **Figure 2.6 (c),** we created circular cavity of 16 mm at 6 cm from strip edge and water is used as fluid. Result shows 43.9%, 20.45% and 4.76% decrease in flow rate as compared to strips without cavity and with cavity of 8 mm and 12 mm, respectively. Also, we compared our experimental results with simulation model, and we got similar results as in our experiments that verifies our experimental results. Next, we changed our fluid and used olive oil to check the behavior of fluid flow in porous media. Here, similar trends were obtained as in the case of water discussed earlier. **Figure 2.6 (d), (e) and (f)** shows comparison of simulation and experimental results of liquid imbibition with time along the strip with circular cavity at 6 cm from strip edge using olive oil. In this case flow rate decreases due to higher viscosity of olive oil as compared to water and also because of adding cavities. In **Figure 2.6 (d)**, circular cavity of 8 mm shows 6.08% decrease in flow

rate as compared to strips without cavity. For a case of 12 mm cavity, 6.6% and 0.59 % decrease in flow rate as compared to strips without cavity and with cavity of 8 mm, respectively, was attained as shown in **Figure 2.6 (e)**. As the cavity size is increased to 16 mm, 7.2%, 1.12% and 0.53% decrease in flow rate as compared to strips without cavity and with a cavity of 8 mm and 12 mm, respectively, was obtained [See. **Figure 2.6 (f)**].

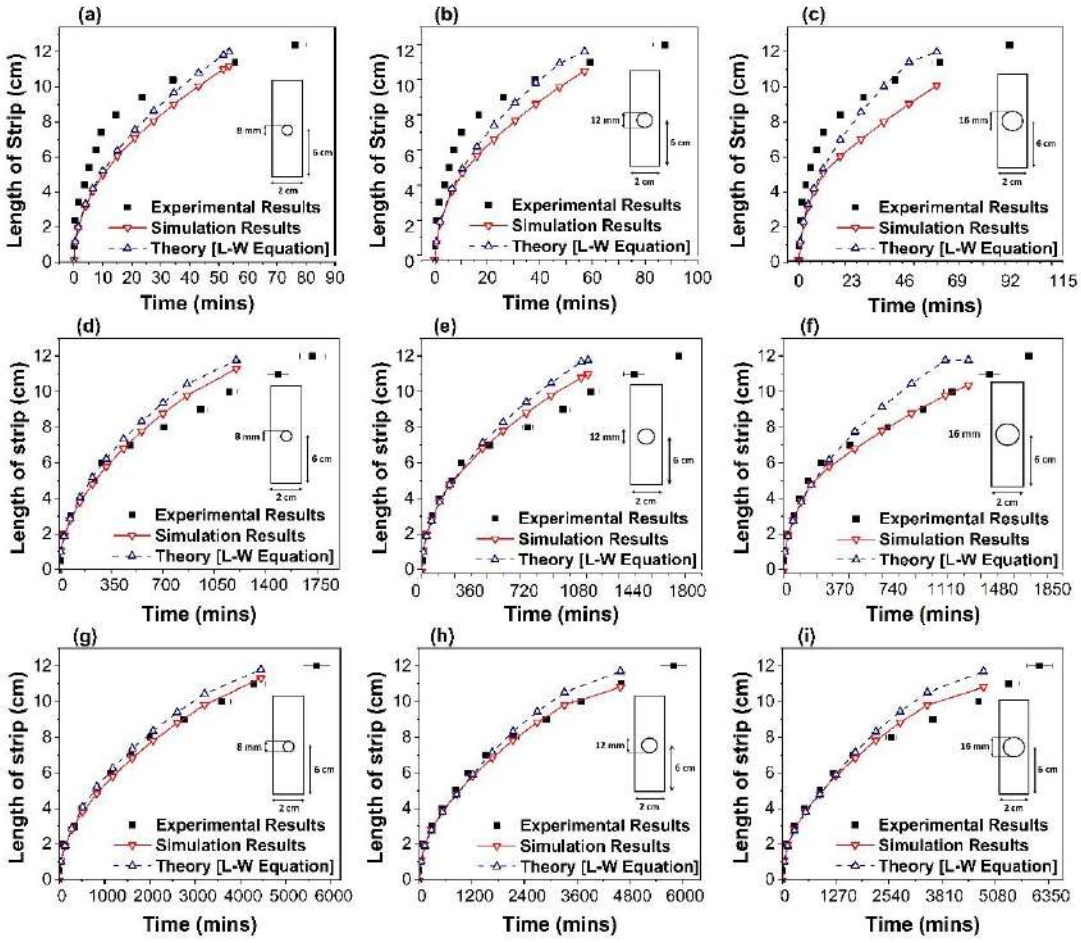

Figure 2.6: Liquid imbibition with time along the strip with circular cavity at the strip center using different liquids used as imbibing liquid. (a-c) Water, (d-f) olive oil, (g-i) castor oil.

Figure 2.6 (g), (h) and (i) shows comparison of simulation and experimental results of liquid imbibition with time along the strip with circular cavity at 6 cm from strip edge using castor oil. In **Figure 2.6 (g)**, in case of circular cavity of 8 mm 3.5 % decrease in flow rate as compared to strips without cavity was attained. For a case of 12 mm cavity, 5.8 % and 2.23 % decrease in flow rate as compared to strips without cavity and with cavity of 8 mm,

respectively, was attained as shown in **Figure 2.6 (h)**. As the cavity size is increased to 16 mm, 11.9%, 8.12% and 5.75% decrease in flow rate as compared to strips without cavity and with a cavity of 8 mm and 12 mm, respectively, was obtained [See. **Figure 2.6 (i)**].

Therefore, as the number of circular cavities in porous media are increased, it provides more resistance in flow of liquid. Furthermore, as we increase the size of cavity it provides more resistance in liquid imbibition. Thus, liquid imbibition rate was decreased.

2.4.2 Effect of changing position of cavities

We also explored the effect of changing the position of circular cavities in paper strips. **Figure 2.7** shows the experimental and simulation results of liquid imbibition with time along the strip with circular cavity at 3 cm from strip edge using different liquids. Here, we changed the position of our cavity from 6 cm to 3 cm from strip edge. **Figure 2.7 (a)** shows the experimental and simulation results of liquid imbibition with time along the strip with circular cavity of diameter 8 cm using water. In this case, to the flow rate decreased by 13.4% as compared to the 8 mm cavity at 6 cm from strip edge. Similarly, we got 10.5 % decrease by using a 12 mm cavity, and 16 % decrease by using 16 mm cavity located at 3 cm from strip edge [See. **Figure 2.7 (b) and (c)**] compared to the corresponding size of cavity located at 6 cm from strip edge.

Figure 2.7 (d), (e) and **(f)** shows the experimental and simulation results of liquid imbibition rate along the strip with circular cavity at 3 cm from the strip edge using olive oil. **Figure 2.7 (d)** shows a decrease of 1.59% as compared to the 8 mm cavity at 6 cm from strip edge. Similarly, we got 1.88 % decrease by using a 12 mm cavity, and 30.8 % decrease by using 16 mm cavity located at 3 cm from strip edge [See. **Figure 2.7 (e) and (f)**] compared to the corresponding size of cavity located at 6 cm from strip edge.

Figure 2.7 (g), (h) and (i) shows the experimental and simulation results of liquid imbibition rate along the strip with circular cavity at the strip 3 cm from the strip edge using castor oil.

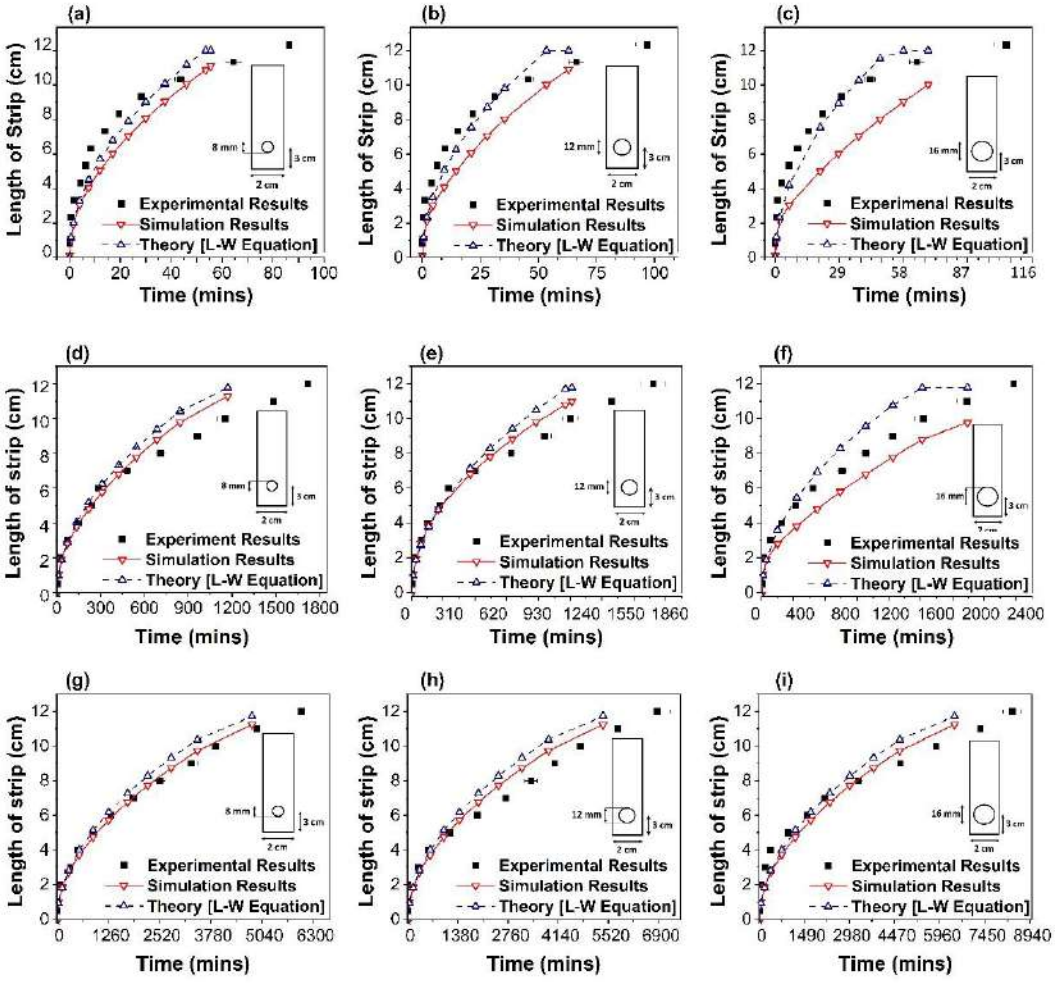

Figure 2.7: Liquid imbibition with time along the strip with circular cavity at the strip bottom using different liquids as imbibing liquid. (a-c) Water, (d-f) olive oil, (g-i) castor oil.

Figure 2.7 (g) shows a 5.87% decrease as compared to the 8 mm cavity at 6 cm from strip edge. Similarly, we got 18.39 % decrease by using a 12 mm cavity, and 36.3 % decrease in flow rate by using 16 mm cavity located at 3 cm from strip edge was attained [See. **Figure 2.7 (h) and (i)**] compared to the corresponding size of cavity located at 6 cm from strip edge. As we create cavity in strip it disturbs pressure gradient that affects the flow. The affected pressure gradient slows the removal of air from the strip boundary 3 (boundary parallel and away from reservoir contact boundary). Moreover, the position of the cavity on strip impacts the flow greatly when it is far from boundary 3 making air removal difficult. As the removal process of air slows, it provides more resistance and the wicking

time increases. Therefore, flow rate decreases by shifting the location of cavities nearer to the strip edge as it provides more resistance from the start of flow.

2.4.3 Experimental comparison with cavities using different liquids

Figure 2.8 shows the experimental results of liquid imbibition with time along the strip length with cavity using water, olive oil and castor oil. **Figure 2.8 (a)** shows the experimental results of liquid imbibition rate along the strip length with a cavity at 6 cm from the strip edge with diameter of 8 mm using water, olive oil and castor oil. This is the simple comparison between different liquids which shows that we get maximum flow time along the length of strip in case of castor oil as compared to olive oil and water due to high viscosity of castor oil. Castor oil is 3.35 times slower than olive oil.

Figure 2.8 (b) shows the experimental results of liquid imbibition rate along the strip length with a cavity at 6 cm from the strip edge with diameter of 12 mm using water, olive oil and castor oil. Olive oil is 19.4 times slower than that of water. Castor oil is 66 times slower than water and 3.4 times slower than olive oil. **Figure 2.8 (c)** shows the experimental results of liquid imbibition with time along the strip length with cavity at 6 cm from the strip edge having diameter of 16 mm using water, olive oil and castor oil. Olive oil is 16.8 times slower than that of water. Castor oil is 60.3 times slower than water and 3.6 times slower than olive oil. **Figure 2.8 (d), (e) and (f)** shows the experimental results of liquid imbibition with time along the strip length with cavity at 4.5 cm from the strip edge with diameter of 8 mm, 12 mm and 16 mm using water, olive oil and castor oil. **Figure 2.8 (d)** indicates that castor oil is 70.62 times slower than water and 3.4 times slower than olive oil. **Figure 2.8 (e)** indicates that castor oil is 71.5 times slower than water and 3.8 times slower than olive oil. **Figure 2.8 (f)** the time required to flow the castor oil to the length of strip is 66 times slower than water and 3.7 times slower than olive oil.

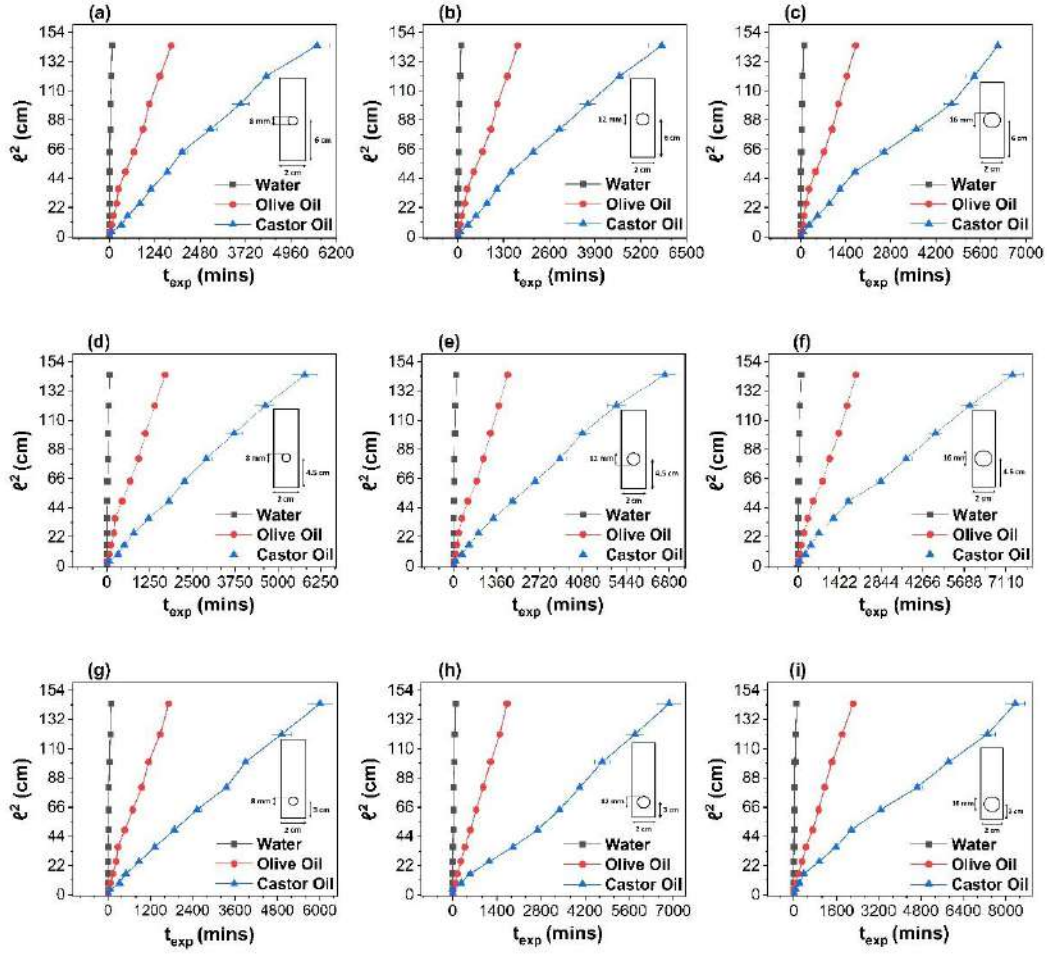

Figure 2.8: Experimental results of liquid imbibition with time along the strip length with cavity using different liquids.

Figure 2.8 (g), (h) and (i) shows the experimental results of liquid imbibition with time along the strip length with cavity at 3 cm from the strip edge with diameter of 8 mm, 12 mm and 16 mm using water, olive oil and castor oil. From **Figure 2.8 (g),** we noticed that water is 20.7 times faster than olive oil and castor oil is 3.5 times faster than olive oil. In **Figure 2.8 (h),** we noticed that olive oil is 0.048 times slower than water. **Figure 2.8 (i),** (16mm circular and 3 cm from strip edge) experimental data showed that castor oil is 85 times slower than water and 3.7 times slower than olive oil. Because of large cavity size provides more resistance in flow and high viscosity fluids required more time to flow.

Figure 2.8 (g), (h) and (i) shows the experimental results of liquid imbibition with time along the strip length with cavity at 3 cm from the strip edge with diameter of 8 mm, 12 mm and 16 mm using water, olive oil and castor oil. From **Figure 2.8 (g),** we noticed that water is 20.7 times faster than olive oil and castor oil is 3.5 times slower than olive oil. In **Figure 2.8 (h),** we noticed that olive oil is 0.048 times slower than water. **Figure 2.8 (i),** (16mm circular and 3 cm from strip edge) experimental data showed that castor oil is 85 times slower than water and 3.7 times slower than olive oil. Because of large cavity size provides more resistance in flow and high viscosity fluids required more time to flow. Straight lines show that ℓ still varies as $t^{1/2}$ for all the cases.

2.4.4 Comparison with theoretical model

In **Figure 2.9 (a)**, t* is the ratio of experimental time and theoretical time from the Lucas-Washburn equation ($t^* = t_{exp}/t_{L\text{-}W}$). The ratio of location of the cavity (L) to the length of the strip (ℓ) was varied while the ratio of cavity diameter (d) to strip width (w) was kept constant. $L/\ell \approx 1$ corresponds to cavity located centered at the strip top edge while $L/\ell \approx 0$ corresponds to strip bottom edge. The graph shows that we got a maximum of~1.9 times decrease in flow ambition time at $L/\ell \approx 0.2$ compared with Lucas-Washburn equation in

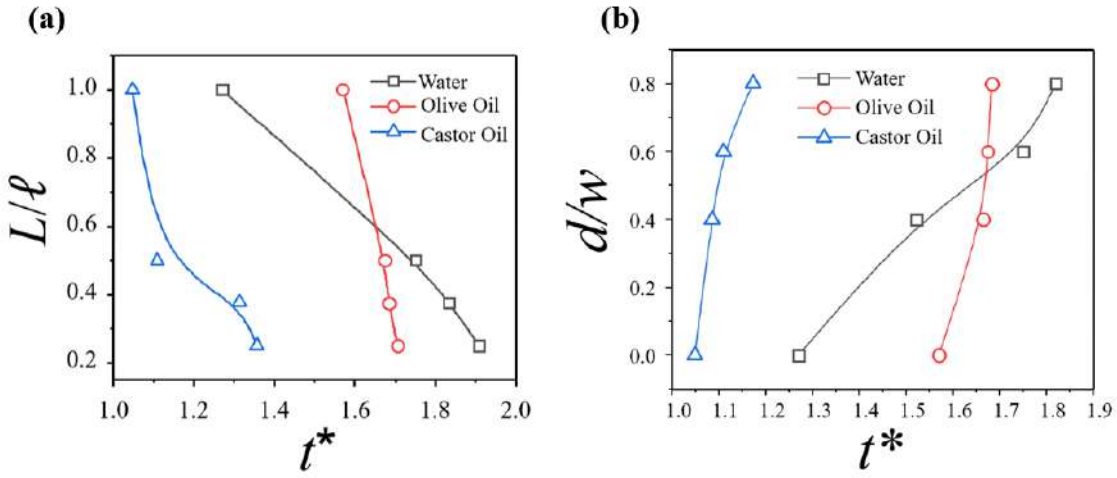

Figure 2.9: Comparison of decrease in flow rate compared with Lucas-Washburn Equation (eqn. 2.7). Here, t^* ($= t_{exp}/t_{L\text{-}W}$) is the ratio of experimental time and theoretical time, L is location of cavity, ℓ is length of strip, d is size of cavity and w is width of strip. **(a)** By changing the ratio L/ℓ and keeping d/w = 0.6, **(b)** By changing the ratio d/w and keeping $L/\ell = 0.5$.

case of water. Similarly, we got ~1.7 times and ~1.4 times decrease for olive oil and castor oil, respectively. d/w was kept constant at 0.6. Thus, smaller the value of L/ℓ, larger will be the flow imbibition time.

In **Figure 2.9 (b)**, we got a maximum of~1.85 times decrease in flow ambition time at d/w ≈ 0.8 compared with Lucas-Washburn equation in case of water. Similarly, we got ~1.6 times and ~1.2 times decrease for olive oil and castor oil, respectively. L/ℓ was kept constant at 0.5 Thus, larger the value of d/w, larger will be the flow imbibition time.

2.5 Conclusion

In this research, we have used circular cavities of different sizes located at different locations of the paper channel with an aim to provide a new method for better flow control and resolution in microfluidic paper-based analytical devices (μPADs). The flow imbibition time is measured using experimental and simulation approaches. We have used three different liquids to explore a variable range of fluidic properties on Whatman grade 42 filter paper. We found that flow imbibition time scales can be decreased to large extent depending on the size and location of the cavities. We attained almost 2 times decrease in flow time compared with Lucas-Washburn (L-W) for water having 16 mm cavity nearer the strip bottom edge at the distance of 3 cm. The more the cavity is located nearer to the strip bottom edge, the more flow resistance it offers. On the other hand, the larger the size of the cavity, the larger is the flow resistance. Overall, we attained a maximum delay in the case of castor oil which was almost 85 times slower than water and 3.7 times slower than olive oil. We found that despite the creation of channel cavities the flow length ℓ still scales as $\approx t^{1/2}$ for all the cases.

We believe that our results will be useful for better flow resolution and control in future porous media-based devices/indictors. Moreover, we have provided an extensive experimental data that can be used for future applications and mathematical modeling.

References

[1] Y. Goossens, A. Wegner, and T. Schmidt, “Sustainability Assessment of Food Waste Prevention Measures: Review of Existing Evaluation Practices,” Front Sustain Food Syst, vol. 3, p. 90, Oct. 2019, doi: 10.3389/FSUFS.2019.00090/BIBTEX.

[2] A. Prajwal, P. Vaishali, zade payal, and D. Sumit, “Food Quality Detection and Monitoring System,” in 2020 IEEE International Students’ Conference on Electrical,Electronics and Computer Science (SCEECS), IEEE, Feb. 2020, pp. 1–4. doi: 10.1109/SCEECS48394.2020.175.

[3] A. Pavelková, “Time temperature indicators as devices intelligent packaging,” Acta Universitatis Agriculturae et Silviculturae Mendelianae Brunensis, vol. 61, no. 1, pp. 245–251, Apr. 2013, doi: 10.11118/actaun201361010245.

[4] “Pharmacy Journal | Pharmaceutical Journal | The Pharma Innovation Journal.” https://www.thepharmajournal.com/ (accessed Jun. 05, 2023).

[5] S. Wang, X. Liu, M. Yang, Y. Zhang, K. Xiang, and R. Tang, “Review of Time Temperature Indicators as Quality Monitors in Food Packaging,” Packaging Technology and Science, vol. 28, no. 10, pp. 839–867, Oct. 2015, doi: 10.1002/pts.2148.

[6] Y. Song et al., “Recyclable Time–Temperature Indicator Enabled by Light Storage in Particles,” Adv Opt Mater, vol. 11, no. 8, Apr. 2023, doi: 10.1002/adom.202202654.

[7] E. Noviana et al., “Microfluidic Paper-Based Analytical Devices: From Design to Applications,” Chem Rev, vol. 121, no. 19, pp. 11835–11885, Oct. 2021, doi: 10.1021/acs.chemrev.0c01335.

[8] Anushka, A. Bandopadhyay, and P. K. Das, “Paper based microfluidic devices: a review of fabrication techniques and applications,” The European Physical Journal Special Topics 2022, pp. 1–35, Dec. 2022, doi: 10.1140/EPJS/S11734-022-00727-Y.

[9] S. Nishat, A. T. Jafry, A. W. Martinez, and F. R. Awan, “Paper-based microfluidics: Simplified fabrication and assay methods,” Sens Actuators B Chem, vol. 336, p. 129681, Jun. 2021, doi: 10.1016/j.snb.2021.129681.

[10] Y. J. Jeong, J. H. Kim, H. J. Ju, and D. S. Kim, “Development of a fully biocompatible and solid enzymatic-time-temperature indicator for cold chain system,” Molecular Crystals and Liquid Crystals, pp. 1–9, Jan. 2023, doi: 10.1080/15421406.2022.2164653.

[11] L. Wang et al., “Time-temperature indicators based on Lipase@Cu3(PO4)2 hybrid nanoflowers,” LWT, vol. 168, p. 113857, Oct. 2022, doi: 10.1016/j.lwt.2022.113857.

[12] R. Kumar Jaiswal, S. Kumar Mendiratta, S. Talukder, A. Soni, B. Lal Saini, and C. Rohit Kumar Jaiswal, “Enzymatic time temperature indicators: A review,” ~ 643 ~ The Pharma Innovation Journal, vol. 7, no. 10, pp. 643–647, 2018, Accessed: Jun. 06, 2023. [Online]. Available: www.thepharmajournal.com

[13] A. T. Jafry, H. Lim, W.-K. Sung, and J. Lee, “Flexible time–temperature indicator: a versatile platform for laminated paper-based analytical devices,” Microfluid Nanofluidics, vol. 21, no. 3, p. 57, Mar. 2017, doi: 10.1007/s10404-017-1883-x.

[14] T. Gao, Y. Tian, Z. Zhu, and D.-W. Sun, “Modelling, responses and applications of time-temperature indicators (TTIs) in monitoring fresh food quality,” Trends Food Sci Technol, vol. 99, pp. 311–322, May 2020, doi: 10.1016/j.tifs.2020.02.019.

[15] J. F. Artiola and M. L. Brusseau, “The Role of Environmental Monitoring in Pollution Science,” Environmental and Pollution Science, pp. 149–162, 2019, doi: 10.1016/B978-0-12-814719-1.00010-0.

[16] T. Lu, X. Chen, and W. Bai, “Research on environmental monitoring and control technology based on intelligent Internet of Things perception,” The Journal of Engineering, vol. 2019, no. 23, pp. 8946–8950, Dec. 2019, doi: 10.1049/joe.2018.9154.

[17] A. W. Martinez, S. T. Phillips, M. J. Butte, and G. M. Whitesides, “Patterned Paper as a Platform for Inexpensive, Low-Volume, Portable Bioassays,” Angewandte Chemie International Edition, vol. 46, no. 8, pp. 1318–1320, Feb. 2007, doi: 10.1002/anie.200603817.

[18] Lim, Jafry, and Lee, “Fabrication, Flow Control, and Applications of Microfluidic Paper-Based Analytical Devices,” Molecules, vol. 24, no. 16, p. 2869, Aug. 2019, doi: 10.3390/molecules24162869.

[19] J. Cottet and P. Renaud, “Introduction to microfluidics,” in Drug Delivery Devices and Therapeutic Systems, Elsevier, 2021, pp. 3–17. doi: 10.1016/B978-0-12-819838-4.00014-6.

[20] A. T. Jafry, H. Lim, S. Il Kang, J. W. Suk, and J. Lee, “A comparative study of paper-based microfluidic devices with respect to channel geometry,” Colloids Surf A Physicochem Eng Asp, vol. 492, pp. 190–198, Mar. 2016, doi: 10.1016/j.colsurfa.2015.12.033.

[21] E. W. Washburn, “The Dynamics of Capillary Flow,” Physical Review, vol. 17, no. 3, p. 273, Mar. 1921, doi: 10.1103/PhysRev.17.273.

[22] A. Hasan, B. Foss, and S. Sagatun, “Flow control of fluids through porous media,” Appl Math Comput, vol. 219, no. 7, pp. 3323–3335, Dec. 2012, doi: 10.1016/j.amc.2011.07.001.

[23] S. G. Jeong, J. Kim, S. H. Jin, K. S. Park, and C. S. Lee, “Flow control in paper-based microfluidic device for automatic multistep assays: A focused minireview,” Korean Journal of Chemical Engineering, vol. 33, no. 10, pp. 2761–2770, Oct. 2016, doi: 10.1007/S11814-016-0161-Z/METRICS.

[24] A. Satter and G. M. Iqbal, “Fundamentals of fluid flow through porous media,” in Reservoir Engineering, Elsevier, 2016, pp. 155–169. doi: 10.1016/B978-0-12-800219-3.00009-7.

[25] P. Mehrdel, H. Khosravi, S. Karimi, J. A. L. Martínez, and J. Casals-Terré, “Flow Control in Porous Media: From Numerical Analysis to Quantitative μPAD for Ionic

Strength Measurements," Sensors, vol. 21, no. 10, p. 3328, May 2021, doi: 10.3390/s21103328.

[26] Lim, Jafry, and Lee, "Fabrication, Flow Control, and Applications of Microfluidic Paper-Based Analytical Devices," Molecules, vol. 24, no. 16, p. 2869, Aug. 2019, doi: 10.3390/molecules24162869.